

RXTE All-Sky Monitor Detection of the Orbital Period of Scorpius X-1

Keith W. Vanderlinde, Alan M. Levine, and Saul A. Rappaport

Department of Physics and Center for Space Research

Massachusetts Institute of Technology

Room 37-575, 77 Massachusetts Ave., Cambridge, MA 02139

aml@space.mit.edu

ABSTRACT

The orbital period of Scorpius X-1 has been accepted as 0.787313 d since its discovery in archival optical photometric data by Gottlieb, Wright & Liller (1975). This period has apparently been confirmed multiple times in the years since in both photometric and spectroscopic optical observations, though to date only marginal evidence has been reported for modulation of the X-ray intensity at that period. We have used data taken with the All Sky Monitor on board the *Rossi X-Ray Timing Explorer* over the past 6 years to search for such a modulation. A major difficulty in detecting the orbit in X-ray data is presented by the flaring behavior in this source, wherein the (1.5-12 keV) X-ray intensity can change by up to a factor of two within a fraction of a day. These flares contribute nearly white noise to Fourier transforms of the intensity time series, and thereby tend to obscure weak modulations, i.e., of a few percent or less. We present herein a new technique for substantially reducing the effects of the flaring behavior while, at the same time, retaining much of any periodic orbital modulation, provided only that the two temporal behaviors exhibit different spectral signatures. Through such a search, we have found evidence for orbital modulation at the $\sim 1\%$ level with a period of 0.78893 d, equal within our accuracy to a period which differs by 1 cycle per year from the accepted value. If we compare our results with the period of the 1 year sideband cited by Gottlieb et al. we conclude that the actual period may in fact be 0.78901 d. Finally, we note that many of the reported optical observations of Sco X-1 have been made within one or two months of early June, when Sco X-1 transits the meridian at midnight. All periodicity searches based only on such observations would have been subject to the same 1 cycle per year alias that affected the search of Gottlieb, Wright, & Liller (1975).

Subject headings: binaries: close—stars: individual (Sco X-1)—X-rays: binaries

1. Introduction

Scorpius X-1 is the most prominent of the bright Galactic bulge X-ray sources. These are persistent, high-luminosity X-ray sources located in directions more or less towards the Galactic center, and are typified by, in addition to Sco X-1, GX340+0, GX349+2, GX3+1, GX5–1, GX9+1, GX9+9, GX13+1, and GX17+2. The 2 to 10 keV intensities of these sources are often seen to vary within a range limited to about a factor of two or so; much larger changes in strength are rare. Neither eclipses nor persistent periodic pulsations have been detected in any of them. These sources are believed to be low-mass X-ray binaries (LMXBs), binaries with short orbital periods in which accretion onto a neutron star primary is fed by Roche lobe overflow from a companion less massive than the Sun. Two classes of LMXBs, the “Z” and “atoll” types, are distinguished by distinctive tracks seen in X-ray color-color diagrams. In both types of source, the overall intensity and features of Fourier power density spectra, including quasiperiodic oscillations, also change in a characteristic way with location along the color-color track (Hasinger & van der Klis 1989; van der Klis 2000). The brightest bulge sources are of the Z-type, which may be emitting close to the Eddington limit for a neutron star of mass $\sim 1.4 M_{\odot}$. Although Sco X-1 is by far the brightest persistent source, it is not likely to be intrinsically more luminous than the other Z sources; rather it is thought to be ~ 3 times closer than most of the bulge sources (Bradshaw, Fomalont, & Geldzahler 1999).

Sco X-1 exhibits only the so-called normal and flaring branches of the Z-source X-ray color-color diagram; it does not exhibit a “horizontal branch” (Hasinger & van der Klis 1989). During frequent excursions onto the flaring branch, the source intensity increases by up to a factor of ~ 2 . These flares often come and go on time scales of hours (Bradt et al. 1975, and references therein).

The high level of activity that Sco X-1 displays in X-rays also appears in the optical and radio bands where the variability is correlated with the variability in the X-ray band (Sandage et al. 1966; Bradt et al. 1975; Canizares et al. 1975; Wright, Gottlieb, & Liller 1975). In the optical, it ranges over blue magnitudes of 11.8 to 13.6, but on time scales of 1 day or less it rarely changes by more than 1 magnitude.

Apart from strong X-ray emission and occasional weak radio emission, the binary nature of the bright Galactic bulge sources is only subtly, if at all, manifested observationally. Of the 9 sources listed above, orbital periods have been determined for only Sco X-1, GX 9+9, and, possibly, GX349+2 (Gottlieb, Wright & Liller 1975, hereafter GWL; Hertz & Wood 1988; Schaefer 1990; Wachter & Margon 1996).

The orbital period of Sco X-1 was first found by GWL in a search for periodicities in

85 years of photometric optical data obtained from plates in the Harvard collection. GWL found four distinct candidates for the orbital period, viz., 0.787313 d, 0.78901 d, 0.81069 d, and 3.74001 d. They identified 0.787313 d as the likely orbital period, while the other periods were explained as one year, one month, and one day sidebands, respectively, i.e., as artifacts of the limited coverage of the observations. Use of a large number of measurements was critical to GWL’s success in elucidating these periodicities against the background of high frequency noise from random variations in brightness; in the optical the orbital modulation has a full amplitude of only ~ 0.2 magnitude (Gottlieb, Wright, & Liller 1975; Wright, Gottlieb, & Liller 1975).

Cowley & Crampton (1975) carried out spectroscopic observations of Sco X-1 and found radial velocity variations in the He II and H emission lines with a period of 0.787 ± 0.006 d and thereby conclusively demonstrated the orbital nature of the 0.787 day variations. If the emission lines are formed, e.g., in an accretion disk around the X-ray emitting star, then the epoch of minimum brightness found by GWL corresponds to superior conjunction of the X-ray source (Cowley & Crampton 1975; Crampton et al. 1976).

The presence of a 0.787 d period has been confirmed in a number of other studies based on optical photometry (e.g., van Genderen 1977; see Augusteijn et al. 1992) or on radial velocities obtained from optical spectroscopy (e.g., Bord et al. 1976; LaSala & Thorstensen 1985). Further information on the binary system has recently been obtained by Steeghs & Casares (2002), who used optical spectroscopy to uncover evidence of the donor star in the binary system and to obtain estimates of its radial velocity amplitude.

No significant periodicity at 0.787313 d or any nearby period in the X-ray flux from Sco X-1 has been reported. Priedhorsky & Holt (1987) searched for a signal at the GWL period in 5 years of 3-6 keV intensity measurements from the All-Sky Monitor on *Ariel V* and found only a weak modulation with an amplitude of $\sim 0.4\%$. Priedhorsky & Holt did not report any investigations of variability at other periods.

We have analyzed X-ray intensities of Sco X-1 recorded over more than six years by the All Sky Monitor (ASM) on board the *Rossi X-ray Timing Explorer*, and have found evidence of a periodicity with a period of 0.78893 d. This period is consistent with GWL’s 0.78901 d period, and we therefore tentatively propose that the latter value is the orbital period of Sco X-1, while the 0.787313 d period is a one-year sideband produced as a consequence of the observational window function.

2. Observations

The ASM comprises 3 coded-aperture cameras, or Scanning Shadow Cameras (SSCs), mounted as an assembly that can be rotated around a single axis by a motorized drive (Levine et al. 1996). The shadow pattern data from each 90-second exposure with a single SSC are analyzed to obtain intensity estimates of each pre-cataloged source that is within the field of view. The analysis is done for the overall energy band of the ASM, $\sim 1.5\text{-}12$ keV, as well as the nominal 1.5-3 keV, 3-5 keV, and 5-12 keV bands (the A, B, and C bands, respectively).

Our analysis involves both intensities and colors, i.e., ratios of intensities from different energy bands. We utilized the intensities produced as part of the standard processing done by the *RXTE* ASM team (Levine et al. 1996). In the derivation of these intensity estimates, corrections are made for instrumental characteristics which have changed over time. The correction factors are constructed to remove trends in the derived intensities of the Crab Nebula (including the pulsar) over the course of the mission and to remove any dependence on SSC, position in the field of view, etc. The factors obtained for the Crab Nebula are also applied to other sources even though this is an approximation that becomes less accurate as the source spectrum deviates more strongly from that of the Crab. One may therefore expect some systematic errors in the intensities of Sco X-1 since its spectrum is not the same as that of the Crab; these are expected to be small in the intensities derived from SSC 2 and larger in the intensities derived from SSCs 1 and 3. The gas-filled proportional counter detector in SSC 1 has a slow leak that has resulted in the photon energy to pulse height conversion gain increasing at a rate of approximately 9% per year. On one occasion, early in the year 2000, the flight software pulse height intervals that define the individual energy bands of SSC 1 were modified to reduce the effects of the gain changes. For the present analysis, we have made additional empirical corrections to the A and B channel intensities from observations with SSC 1 to remove much of the remaining signature of instrumental gain changes. In SSC 3, 2 of 8 carbon-coated quartz fiber anodes were irretrievably damaged in the first week after launch, and a third anode failed after about 7 months. Gross calibration changes since then have rendered 2 of the remaining 5 anodes unusable. Because of these complications, we do not use data from SSC 3 in the present analysis. In all cases, however, the gain changes and correction factors should not contribute any significant amount of spurious power at temporal frequencies close to 1 cycle d^{-1} where the search for orbital modulations takes place.

Over 11,000 intensity measurements of Sco X-1 have been obtained by each of SSCs 1 and 2 since the ASM began routine operations in late February 1996. The 1.5-12 keV light curve of Sco X-1 using data from SSC 2 only is presented in Figure 1a. The flaring

behavior associated with excursions onto the flaring branch is clearly visible, with frequent and irregular flares above a relatively stable baseline. In Figure 1b we show the hardness ratio $I(5-12 \text{ keV})/I(3-5 \text{ keV})$. Note, in particular, that the hardness ratio increases strongly during the flares (Hasinger & van der Klis 1989; van der Klis 2000).

3. Analysis

In this section we first describe a standard Fourier transform analysis of the time series of X-ray intensity data obtained from Sco X-1. The prominent flaring activity is shown to introduce a significant amount of noise into the transform which will likely mask any signature of a weak orbital modulation. We then introduce a new analysis algorithm which greatly reduces the effects of the flaring behavior. This approach makes use of the strong spectral changes during the flares.

To begin our analysis, the intensities from each of SSCs 1 and 2 were assigned to 0.01-d time bins, and the mean intensity was subtracted from the populated bins. Each resulting linear array was extended by a factor of eight by padding with zeros and was then transformed using a Fast Fourier Transform (hereafter FFT) code. The power at each frequency (the quadratic sum of the real and imaginary parts of the output of the FFT) was divided by the mean power of the entire spectrum. The extension of the linear arrays yields interpolated power density spectra (PDSs) in which the sensitivity for detection of periodicities is more uniform than in an uninterpolated PDS. The results from SSC 2 are shown in Figure 2a, and provide no obvious evidence for any significant periodicity. Even modulations with frequencies close to one cycle per day, which often appear in PDSs of ASM data as a result of the observational window function acting on low-frequency source variability, are not noticeable in the PDS of the raw data. This is taken as evidence that the power density is dominated by the effects of the flares in the intensity of Sco X-1, and thus any small amplitude modulations due to the orbit are likely to be undetectable as well.

In order to significantly reduce the noise power introduced by the flaring behavior and possibly increase the sensitivity for detection of weak modulation at the orbital frequency, we utilize the fact that the intensity of Sco X-1, like other Z sources, exhibits distinct spectral hardening during the flares (see, e.g., Hasinger & van der Klis, 1989). The relation between intensity and spectral hardness from the ASM data set itself is illustrated in Figure 3, where the intensity in each of the A, B, and C bands, which we will denote by I_A , I_B , and I_C , respectively, is plotted vs. the hardness ratio defined as $R_{C,B} = I_C/I_B$. Note that on the average the intensity increases monotonically, though not quite linearly, as $R_{C,B}$ increases. The smooth curves in each panel illustrate models of the spectral behavior of the flares that

we utilize below.

Our flare-suppression algorithm utilizes simple analytic functions to describe the mean intensity–hardness-ratio behavior. These expressions are then used to “correct” the intensity history of Sco X-1 so as to largely remove the flaring behavior. In the following detailed description of the method, we use unprimed symbols to denote quantities that would be observed in the hypothetical *absence* of any modulations due to the orbit, and primed symbols to denote quantities affected by orbital modulations.

We start by defining the *mean* spectral track that would be followed by the source in an intensity–hardness diagram, such as those shown in Figure 3, in the absence of orbital modulations by:

$$\hat{I}_k(t) = F_k [R_{ij}(t)], \quad (1)$$

where $\hat{I}_k(t)$ is the model intensity in the k th energy channel, t is the elapsed time, and F_k describes the shape of the track which is taken to be a function of the hardness ratio in two energy channels i and j :

$$R_{ij}(t) \equiv \frac{I_i(t)}{I_j(t)} \quad (2)$$

with channel i being at higher energies than channel j . Here, the energy channel k whose intensity we are modeling may or may not be the same as channel i or j . The intensities $I_k(t)$, model intensities $\hat{I}_k(t)$, and hardness ratios $R_{ij}(t)$ are defined as those that would be detected if there were no modulations due to the orbit.

When any orbital modulation is defined so as to have a mean value of zero and is small in amplitude, we can still describe the mean intensity–hardness relation using the same function F_k :

$$\hat{I}'_k(t) \simeq F_k [R'_{ij}(t)], \quad (3)$$

where, as stated above, the primes indicate hardness ratios and model intensities affected by orbital modulations. We model the orbital modulation in the k th channel by a simple multiplicative term, $M_k(t)$, to represent a small increase or decrease from the mean in the degree of scattering or absorption out of the line of sight, or scattering into the line of sight. Thus,

$$R'_{ij}(t) \simeq \frac{I_i(t)M_i(t)}{I_j(t)M_j(t)}. \quad (4)$$

A modified data set, $C_k(t)$, approximately corrected for the flaring, is then given by:

$$C_k(t) \equiv \frac{I'_k(t)}{F_k [R'_{ij}(t)]} \simeq \frac{I_k(t)M_k(t)}{F_k [R_{ij}(t)M_i(t)/M_j(t)]}, \quad (5)$$

where the first ratio is expressed in terms of measured quantities (i.e., with the orbital modulation included), and the second ratio is expressed in terms of the intrinsic source behavior.

In order to learn about the properties of the corrected data set, we expand the numerator and denominator in Taylor series about the point $M_i = M_j = 1$, i.e., we take $M(t) = 1 + \delta M(t)$. The above expression can then be written:

$$C_k \simeq \frac{I_k(1 + \delta M_k)}{\left[F_k(R_{ij}) + \left(\frac{\partial F_k}{\partial R'_{ij}} \right)_0 \left(\frac{\partial R'_{ij}}{\partial M_i} \right)_0 \delta M_i + \left(\frac{\partial F_k}{\partial R'_{ij}} \right)_0 \left(\frac{\partial R'_{ij}}{\partial M_j} \right)_0 \delta M_j \right]}, \quad (6)$$

where we have dropped explicit time dependences in the interest of simplicity. After collecting terms and making use of the assumption that the δM 's are small, we find the following simplified expression for the behavior of the corrected data set in the presence of orbital modulations:

$$C_k \simeq \frac{I_k}{F_k(R_{ij})} \left\{ 1 + \delta M_k - \frac{d \ln F_k}{d \ln R_{ij}} [\delta M_i - \delta M_j] \right\}. \quad (7)$$

To the extent that the flaring behavior follows a distinct track in the color–intensity diagram, the factor $I_k/F_k(R_{i,j})$ is nearly constant, i.e., independent of flaring behavior. This factor will also contain some residual random fluctuations in the source intensity that do not follow the color–intensity track, as well as any measurement errors. The factor in curly brackets contains the desired time-dependent orbital modulations, i.e., the δM 's.

From equation (7) one may see that the manifestation of orbital modulations in the corrected data set consists of two parts: (i) the modulation in the channel being corrected, and (ii) a term proportional to the difference in the orbital modulation in the two channels used to define the hardness ratio. There are a couple of noteworthy combinations of terms in this equation. First, if $\delta M_i = \delta M_j$, the modulation appearing in C_k is just that of the orbital modulation in the k th energy band being studied. Second, if the energy dependence of the modulations in the different bands accidentally resembles that of the flaring, i.e., $\delta M_k \simeq d \ln F_k / d \ln R_{i,j} (\delta M_i - \delta M_j)$, then the modulations in the corrected data set will have a greatly reduced amplitude, possibly rendering them undetectable.

We have chosen a simple functional form to represent the spectral-intensity changes in the different energy channels of the ASM (also see Figure 3):

$$F_k(R_{i,j}) = \alpha_k + \beta_k R_{i,j}^{\gamma_k}. \quad (8)$$

A table of parameters for the various ASM energy channels is given for reference in Table 1. For this particular functional form we have

$$d \ln F_k / d \ln R_{i,j} = \frac{(F_k - \alpha_k) \gamma_k}{F_k}. \quad (9)$$

Note that $d \ln F_k / d \ln R_{i,j}$ is only approximately constant through the flaring cycle and, in fact, varies by $\pm 7\%$ to $\pm 20\%$, depending on the energy band. Typical values of $d \ln F_k / d \ln R_{i,j}$ for each of the energy bands of SSC 2 are also listed in Table 1.

4. Results

We have applied the hardness-ratio-based correction procedure described above (see, e.g., eq. 5) to each of the energy channels in each of SSCs 1 and 2. The corrected data set for the C channel of SSC 2 is shown as an example in Figure 1c, while the hardness ratios used in the procedure are shown in Fig. 1b. A comparison of the corrected data with the raw data indicates a dramatic reduction in source variability (relative to mean source strength). Corrected data sets from the A and B channels of SSC 2, as well as from all three channels from SSC 1, also have greatly reduced variability.

As was done for the raw data, the corrected data were binned into 0.01-d time bins and the mean value subtracted from those bins containing data. The binned data sets were padded with zeros and then transformed using the FFT. Again, the resulting powers were normalized to the mean power across the spectrum. The results for the C channel of SSC 2 are shown in Figure 2b. Peaks near frequencies of $\sim 1 \text{ cycle d}^{-1}$, related to a window function frequency, are now clearly evident in the PDS.

Amongst the other potentially interesting peaks in the frequency range of 0.5 to 1.75 d^{-1} is one at a frequency corresponding to a period of $0.78893 \pm 0.00010 \text{ d}$. The normalized power reaches a value of 11 close to this frequency, and for an assumed exponential probability distribution, the probability of a statistical fluctuation causing a peak this large in a particular frequency bin is $\sim 2 \times 10^{-5}$. Given that there are roughly 2500 independent frequencies in the range displayed in Fig. 2b, the probability of finding a peak this large in any bin is $\sim 5\%$. Although this is not of great significance by itself, this frequency is actually of *a priori* interest. A blowup of this region of the PDS is shown in Figure 4a. The peak appearing in the SSC 2, channel C data is clearly removed from the frequency corresponding to the GWL period, but it does appear to be coincident with one of the other frequencies identified in the analysis of GWL, i.e., the frequency corresponding to a period of 0.78901 d. In fact, the difference in frequency between the GWL prime frequency and the frequency of the peak we see corresponds to a period of $384 \pm 22 \text{ days}$ – i.e., quite consistent with a 1-year sideband of the GWL period at a frequency corresponding to a period of 0.789014 d ($1.0/0.787313 \text{ d} - 1.0/365.25 \text{ d} = 1.0/0.789014 \text{ d}$).

This peak at 0.78893 d appears with roughly equal amplitude in the A, B, C and summed

(A+B+C) bands (see Fig. 5). Note that, while the data in the three different bands are independent in terms of photon counting statistics, the power in them is dominated by the variability of Sco X-1 whose spectrum does not change by large factors. Thus, the different channels are all similarly affected by both the source variability and the window function. Moreover, the flaring in each of the bands was removed utilizing the same hardness ratio $R_{C,B}$ (not the same functions F_k , however). Thus, the corrected data sets used to produce the PDSs in Fig. 5 do not represent three completely independent sets of observations.

The analysis procedure described above, with the appropriate hardness ratio corrections, was also applied to the data from SSC 1. The results are shown in Figure 4b. The normalized power in the bin that we have identified as the likely orbital frequency of Sco X-1 is 5.7. This is not very statistically significant. In fact, one expects a peak this large by random chance somewhere within the frequency range displayed in Figure 4. Nonetheless, this peak at 0.78895 d is the second highest among the ~ 100 independent frequencies in the plot. We take this as a *weak* confirmation that this particular frequency is interesting. The difference between the peak heights in the transforms of data from the two different cameras is more or less consistent with a signal that is of intermediate strength and therefore at the margin of detectability in each.

We compared the results of the correction procedure described above with other methods of reducing the power from the flaring behavior. The other methods included (i) eliminating those measurements above a specified intensity threshold chosen to be just above a baseline value, e.g., 1050 cts s^{-1} in the 1.5-12 keV band of SSC 2, and (ii) eliminating those measurements with hardness ratios corresponding to typical flaring values, i.e., $R_{C,B} > 1.25$ (see Fig. 3). In general, these other methods yielded smaller peaks close to a period of 0.789014 d than did our correction procedure described above. Combination of our correction procedure with alternative method (ii) resulted in peaks which are comparable in strength to those found without elimination of any measurements.

We carried out two further checks of our analysis of the data from SSC 2. First, we transformed the window function corresponding to the data set from this camera. No interesting peaks were found near the period of Sco X-1. Second, we transformed different subsections of the data to ascertain whether the amplitude of the orbital modulation might be varying with time. Unfortunately, with such a weak signal we are able to say only that the modulation is consistent with having been stronger during the first half of the *RXTE* mission.

We see no interesting harmonic peaks in the PDS at two or three times the frequency of the peak that we have identified.

Next, we estimate the amplitude of the orbital modulation detected in SSC 2. Due to the fact that the data have been corrected by dividing by a function of the hardness ratio, it is not obvious what the Fourier amplitude or a fold, modulo the orbital period, will reveal about the intrinsic amplitude or shape of the orbital modulation. Therefore, we have chosen, somewhat arbitrarily, to calibrate the amplitude scale in the *forward direction* by the following means. We introduce a fictitious orbital modulation at a nearby frequency $f_{cal} = 1.2600 \text{ d}^{-1}$ with a 1% amplitude in all three energy channels by multiplying the actual data from SSC 2 by the factor $1 + 0.01 \sin(2\pi f_{cal}t + \phi)$. The results are shown in the transforms displayed in Figure 5. From a direct comparison of the “calibration” peak and the one at 0.78893 d (1.2675 d^{-1}), we conclude that the orbital modulation amplitude lies in the range $\sim 0.7\% - 1.4\%$. The higher end of this range allows for the possibility that the modulations were present during only half the time of the ASM observations. This is quite consistent with the fact that the peak at 0.78893 d appears broader than the calibration peak by a factor of ~ 2 . Finally, we note that introducing equal calibration amplitude signals into each energy band is equivalent to assuming that the orbital modulations are colorless and that the third term in curly brackets in equation (7) vanishes.

Under the assumption that the amplitudes of the orbital modulations are not strongly dependent on the energy band, we have used a folded light for the corrected SSC 2 data set to determine the time of minimum X-ray intensity. We find that these minima occur at times $t(\text{X-ray minimum}) = \text{MJD } 51334.93 + 0.789014\text{E}$ (MJD = Modified Julian Date = Julian Date – 2,400,000.5). The times of optical photometric minimum are given by GWL as $t(\text{opt. minimum}) = \text{MJD } 40080.63 + 0.787313\text{E}$. On 1999 June 6 (MJD 51335), the GWL ephemeris predicts $t(\text{opt. minimum}) = \text{MJD } 51335.26$ which is 0.33 d or 0.42 cycles after X-ray minimum. Thus, X-ray minimum is coincident with optical photometric maximum within the uncertainty in the phases of the cycles ($\delta\phi \sim 0.1$). However, we point out that equation (7) allows for the possibility of a phase reversal (i.e., by 180°) in the X-ray minimum of a light curve formed from the *corrected* data, depending on the details of the hardness ratio behavior of the orbital modulations.

5. Discussion

We find evidence for a periodicity in the X-ray flux from Sco X-1 with a period of $0.78893 \pm 0.00010 \text{ d}$, and identify this as likely caused by some physical effect producing modulations of the flux at the orbital period. We do not find good evidence for variability at the 0.787313 d period. In fact, GWL found a periodicity at 0.78901 d that is consistent with the period we find in the ASM data, but since they found that periodicity to be $\sim 20\%$

weaker than that at 0.787313 d, they concluded that the latter was the orbital period while the former was the 1-year sideband produced by the observational window function. We suggest rather that the true orbital period is 0.78901 d and that the 0.787313 d period is the 1-year sideband. Unfortunately, we are unable to evaluate quantitatively the likelihood of the sideband appearing stronger in the photometric data than the true modulation frequency since we do not have access to the plate stack data used by GWL.

We note, however, that ASM observations of Sco X-1 are generally available for more than 10 months each year while most ground-based optical observations of Sco X-1 were likely taken within a couple of months of early June when Sco X-1 is nearly opposite from the Sun. Thus, it is likely that the window function of the optical observations analyzed by GWL would have strong components at a 1-year period. We further note that a modulation with a period of 0.78901 d that is in phase with a modulation at 0.787313 d as described by GWL in early June would be difficult for optical observers to distinguish without observations at other times of the year. For example, the two oscillations would be out of phase by only 0.08 cycles in early May or early July. At even earlier or later dates, the phases of the two modulations would gradually drift apart until they came back together (with a difference of 1 cycle) after one year. We can therefore speculate that there were a limited number of optical observations in the set used by GWL that could have differentiated between the two periods.

The difference between the two periods could well have been missed by independent observers who confirmed the GWL period. Although the optical spectroscopic results of Cowley & Crampton (1975) do support the presence of a periodicity, they did not have the frequency resolution to distinguish between the GWL period and a one year sideband. We also expect that the independent measurements of LaSala & Thorstensen (1985) cannot be used to distinguish the GWL period from one which differs by 1 cycle yr^{-1} .

Due to the small observed amplitude of the X-ray orbital modulation in Sco X-1 we are unable to investigate either the detailed shape of the light curve or the spectral character of the modulations. However, it is clear from the lack of higher harmonics in the FFTs and the similarity in amplitudes of the peaks in Fig. 5 that the light curve has no prominent sharp structure nor is it highly energy dependent. Specifically, the modulation cannot be due to photoelectric absorption in ionized matter which would have a much larger effect in the 1.5-3 keV channel than in the 5-12 keV band. As noted in the previous section, the phase of X-ray minimum appears to be 0.42 cycles earlier than that in the optical. Based on any simple picture for scattering or absorption in the system, one would expect the optical and X-ray minima to be roughly coincident, unless the outgoing radiation is affected by structure on the rim of the accretion disk which is fixed asymmetrically in the rotating frame of the

binary. At the low inclination angle that we are likely to be viewing Sco X-1 (e.g., $i \simeq 30^\circ$, Steeghs & Casares 2002) we would not expect this type of effect. Thus, if our orbital period is correct, we have no ready explanation for the phase of X-ray minimum.

In general, the orbital modulation could be due to attenuation of the beam, i.e., scattering or absorption along the line of sight, or to scattering into the line of sight. Possible sources of the scattering and/or absorption could include a stellar wind of the companion, the surface of the companion, a wind from the accretion disk, or an accretion disk corona (see, e.g., Priedhorsky & Holt 1987). If the modulation takes place near the accretion disk, then some asymmetry around the azimuth of the disk, fixed in the rotating frame of the binary, must be present.

If the donor star serves as a source of scattered radiation (see Priedhorsky & Holt 1987), then we can estimate the maximum effect by computing the solid angle subtended by the donor star. The fractional solid angle is given by $\sim 0.053(1+q)^{-2/3}$, where q is the ratio of the mass of the neutron star to that of the donor star. For plausible masses (see Steeghs & Casares 2002) this fraction is $\sim 2\%$. In order for a $\sim 1\%$ orbital modulation to be due to X-rays scattered into the line of sight from the companion star, this would require an implausibly high X-ray albedo of ~ 0.5 .

The accretion disk might afford a larger solid angle for intercepting X-rays and scattering them into the line of sight. For example, an accretion disk with a half opening angle of 10° would subtend at the neutron star a fractional solid angle of $\sim 17\%$. For reasonable X-ray albedos of $\sim 10\%$ for glancing incidence (see below), this could result in some 1.7% of the X-rays emanating from the Sco X-1 system being scattered. If there is some asymmetry around the disk that yields about a factor of two more scattering at some azimuths than others, this could produce a net orbital modulation of $\sim 1\%$.

The X-ray albedo is $\sim 0.5\sigma_e/\sigma_{pe}$, where σ_e is the angle-averaged electron scattering cross section, and σ_{pe} is the energy-dependent photoelectric absorption cross section appropriate for the composition and ionization state of the scattering medium. The exact coefficient depends on the geometry experienced by the incident and emerging X-rays. For material that is of solar composition and nearly unionized, the albedo should scale roughly as $E^{8/3}$; it should be a strongly increasing function of photon energy, E , that reaches $\sim 6\%$ in the middle of the ASM C band. For more highly ionized plasmas, the albedo can be substantially higher and less energy dependent. The latter property would be relevant in trying to model the nearly energy-independent amplitude we find for the orbital modulation.

A small number of X-ray sources that exhibit orbital modulation have been classified as “accretion disk corona” (ADC) sources, e.g., 4U 1822–37 and 4U 2129+47 (see, e.g., White

& Holt 1982). The ADC sources are supposedly viewed nearly edge on, with the direct path of X-rays from the neutron star blocked by an accretion disk. In this case, most of the X-rays detected at the Earth may be scattered by a hot corona located above and below the inner parts of the accretion disk. The orbital modulation of the observed X-ray flux may then be produced by a thickened disk rim that occults the corona to differing degrees as a function of orbital phase (White & Holt 1982). The modulation is typically large enough in amplitude, e.g., $\sim 20\%$ of the average flux, to be easily detectable even outside of the relatively narrow partial eclipse. However, we cannot say whether similar systems observed at much lower inclinations would show modulations at the $\sim 1\%$ level, because (1) the neutron star would be visible and (2) the disk rim would not occult the corona.

Finally, to help establish the correct orbital period in Sco X-1 we urge optical astronomers to search for modulations in the light from or radial velocity of this system as far from June as practicable.

Acknowledgements

The authors thank Bill Liller, Ron Remillard, and Ned Wright for very helpful discussions, and Arnout van Genderen and Jan Lub for providing some of their archival optical data from Sco X-1. Partial support for this research was provided by NASA Contract NAS5-30612 and NASA Grant NAG5-9189.

REFERENCES

- Augusteijn, T., Karatasos, K., Papadakis, M., Paterakis, G., Kikuchi, S., Brosch, N., Leibowitz, E., Hertz, P., Mitsuda, K., Dotani, T., Lewin, W. H. G., van der Klis, M., & van Paradijs, J. 1992, *A&A*, 265, 177
- Bord, D. J., Messina, R. J., Mook, D. E., & Hiltner, A. 1976, *ApJ*, 206, L49
- Bradshaw, C. F., Fomalont, E. B., & Geldzahler, B. J. 1999, *ApJ*, 512, L121
- Bradt, H. V., et al. 1975, *ApJ*, 197, 443
- Canizares, C. R., et al. 1975, *ApJ*, 197, 457
- Cowley, A. P., & Crampton, D. 1975, *ApJ*, 201, L65
- Crampton, D., Cowley, A., Hutchings, J. B., & Kaat, C. 1976, *ApJ*, 207, 907
- Gottlieb, E. W., Wright, E. L. & Liller, W. 1975, *ApJ*, 195, L33

- Hasinger, G., & van der Klis, M. 1989, *A&A*, 225, 79
- Hertz, P. & Wood, K. S. 1988, *ApJ*, 331, 764
- LaSala, J. & Thorstensen, J. R. 1985, *AJ*, 2077, 90
- Levine, A. M., Bradt, H., Cui, W., Jernigan, J. G., Morgan, E. H., Remillard, R., Shirey, R. E., & Smith, D. A. 1996, *ApJ*, 469, L33
- Priedhorsky, W. C., & Holt, S. S. 1987, *ApJ*, 312, 743
- Sandage, A. R., et al. 1966, *ApJ*, 146, 316
- Schaefer, B. E. 1990, *ApJ*, 354, 720
- Steeghs, D., & Casares, J. 2002, *ApJ*, 568, 273
- van der Klis, M. 2000, *ARA&A*, 38, 717
- van Genderen, A. M. 1977, *Astron. Astrophys. Suppl.*, 28, 119
- Wachter, S., & Margon, B. 1996, *AJ*, 112, 2684
- White, N.E., & Holt, S.S. 1982, *ApJ*, 257, 318
- Wright, E. L., Gottlieb, E. W., & Liller, W. 1975, *ApJ*, 200, 171

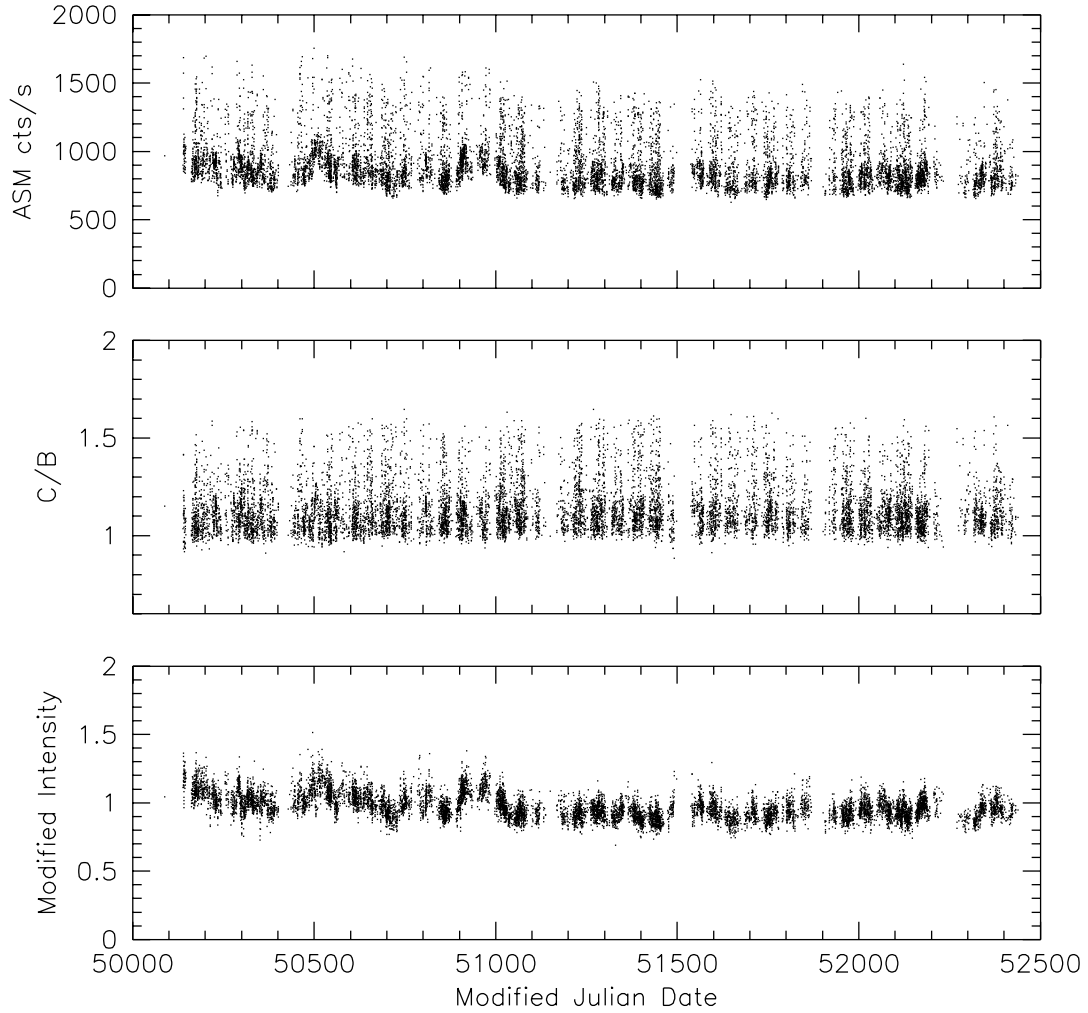


Fig. 1.— (top) The 1.5–12 keV intensity of Sco X-1 from observations made with Scanning Shadow Camera 2 of the *RXTE* ASM. The intensity is the average over each 90 s observation and is given as the count rate that would have been recorded with the source at the center of the field of view of SSC 1 in early 1996. In these units, the intensity of the Crab Nebula is 75 counts s^{-1} . (middle) The hardness ratio, defined as $I(5 - 12 \text{ keV})/I(3 - 5 \text{ keV})$, derived for each SSC 2 observation of Sco X-1. (bottom) Corrected intensity of Sco X-1 from SSC 2 observations (see text).

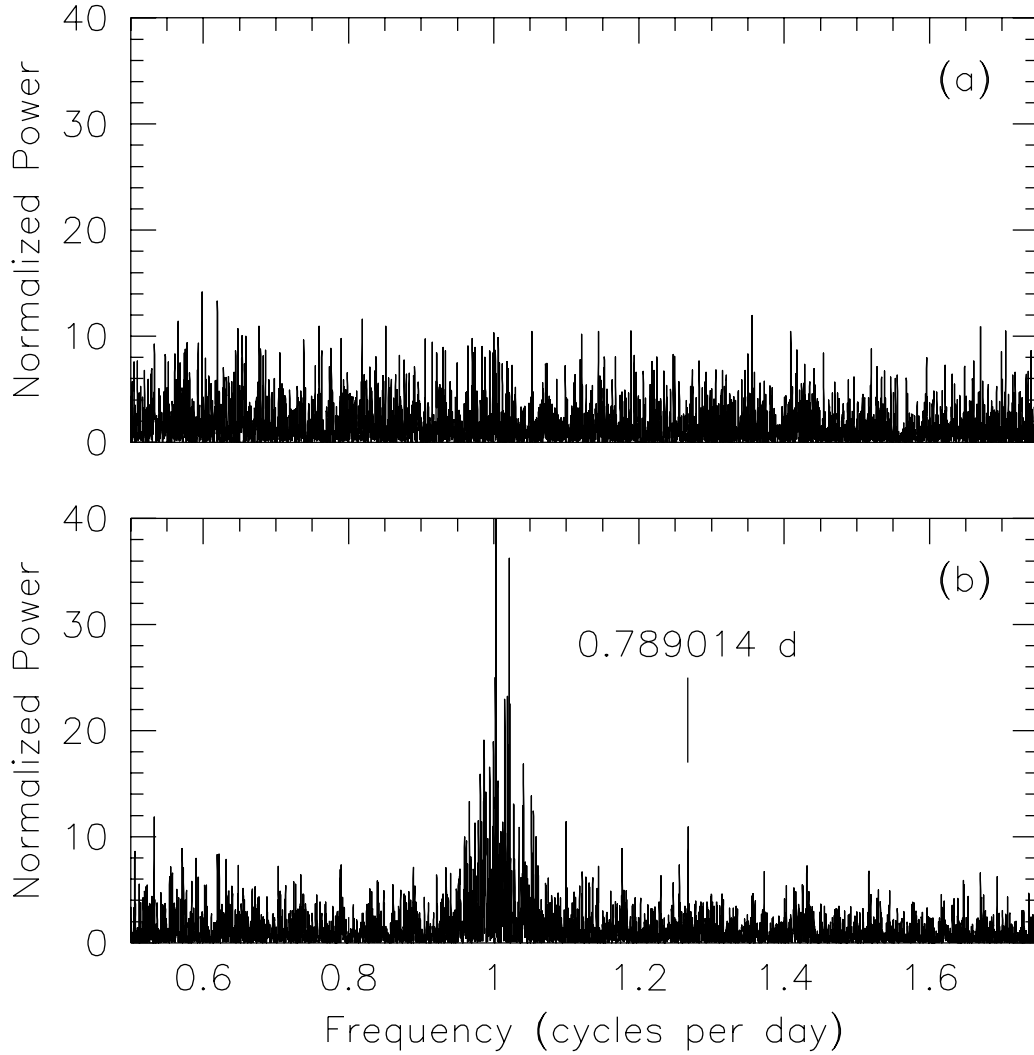


Fig. 2.— (a) Normalized power density spectrum of the uncorrected SSC 2 C band (5-12 keV) data. (b) Normalized power density spectrum of the corrected SSC 2 C band data. A mark indicates the frequency corresponding to a period of 0.789014 days near which there is a peak of interest.

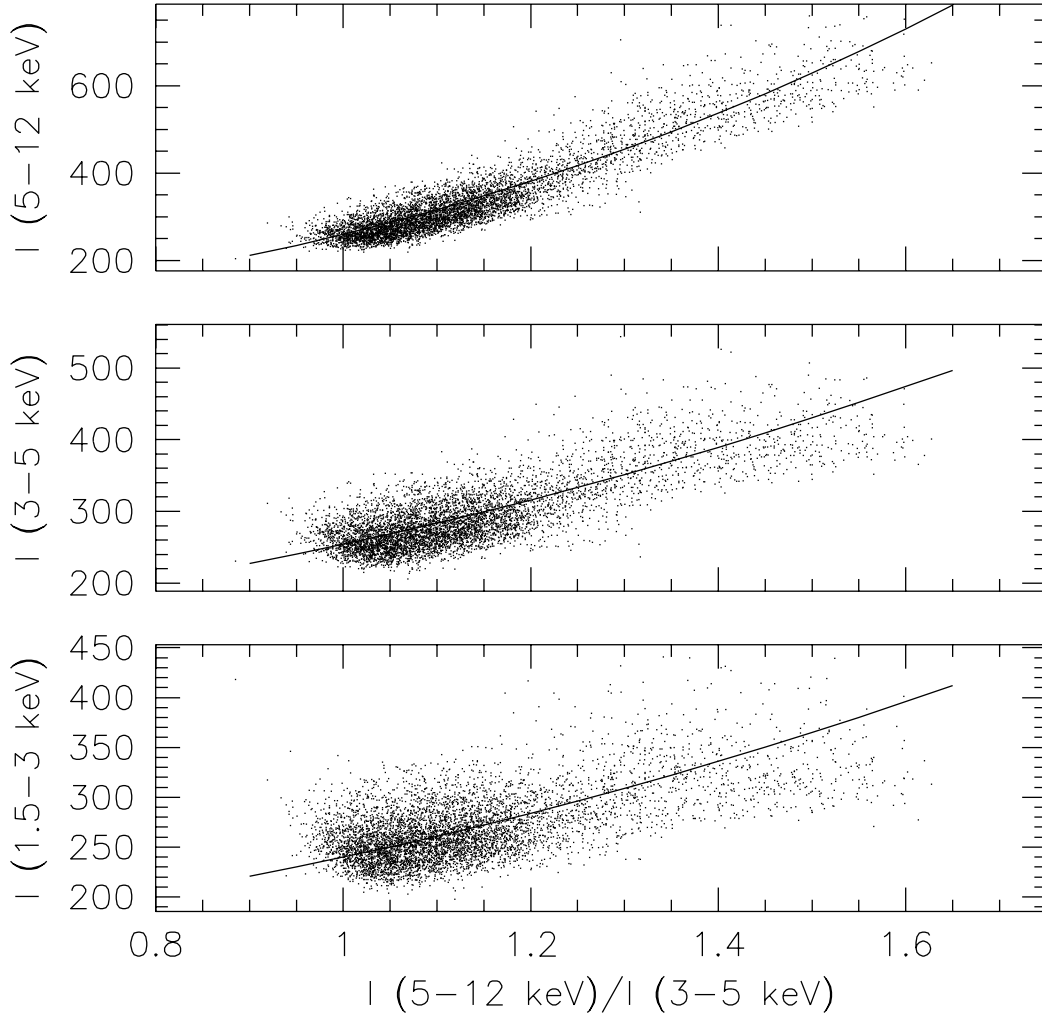


Fig. 3.— (top) SSC 2 C band (5-12 keV) intensities plotted vs. the C band to B band hardness ratio, $R_{C,B}$. (middle) SSC 2 B band (3-5 keV) intensities vs. the hardness ratio. (bottom) SSC 2 A band (1.5-3 keV) intensities vs. the hardness ratio. In all three panels, the solid curve is a model of the mean relation between the intensity and hardness ratio (see eq. 8 and Table 1).

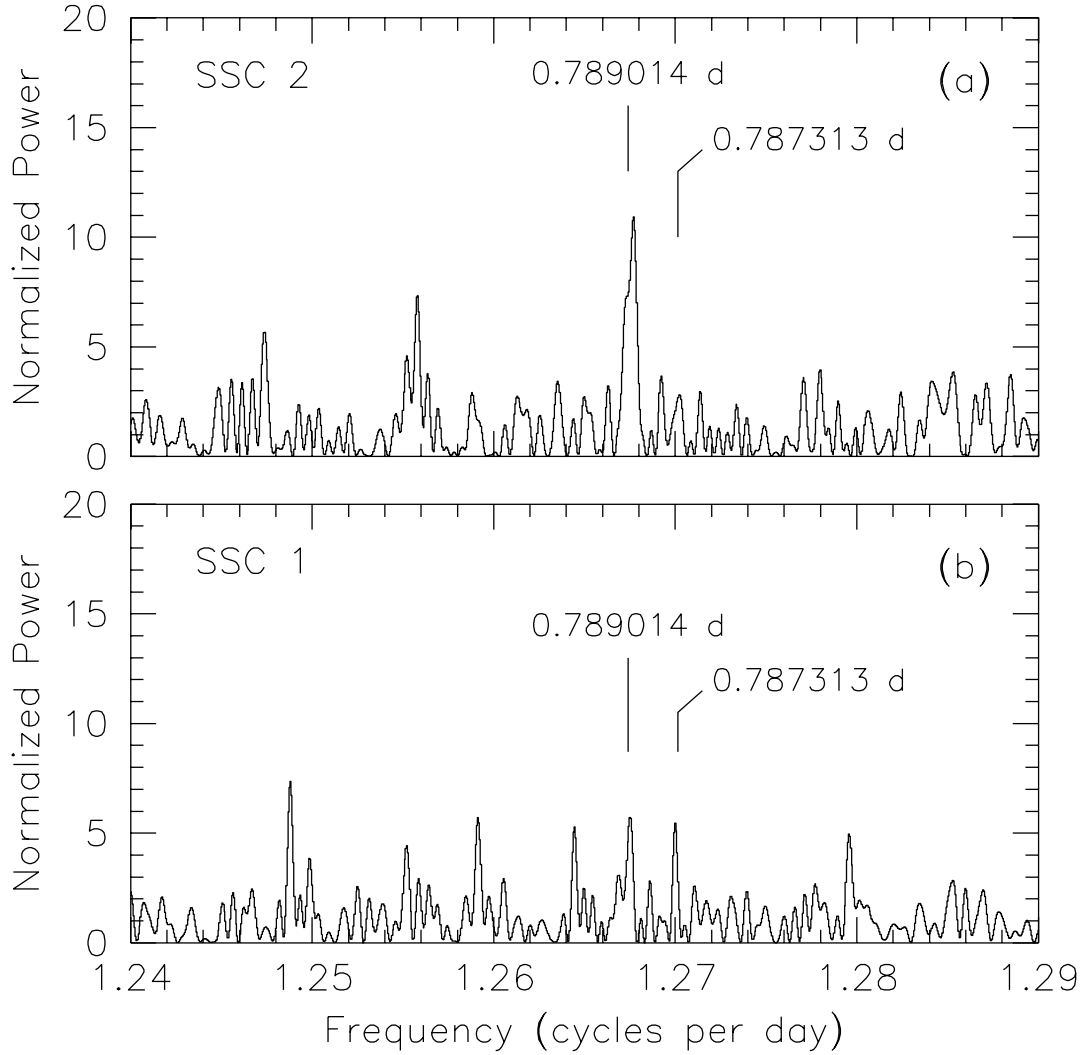


Fig. 4.— (a) Normalized power density spectrum of the corrected SSC 2 C band data in the frequency region around the orbital period of Sco X-1. Marks indicate frequencies corresponding to periods of 0.789014 days and 0.787313 days (GWL's orbital period). (b) Normalized power density spectrum of the corrected SSC 1 C band data.

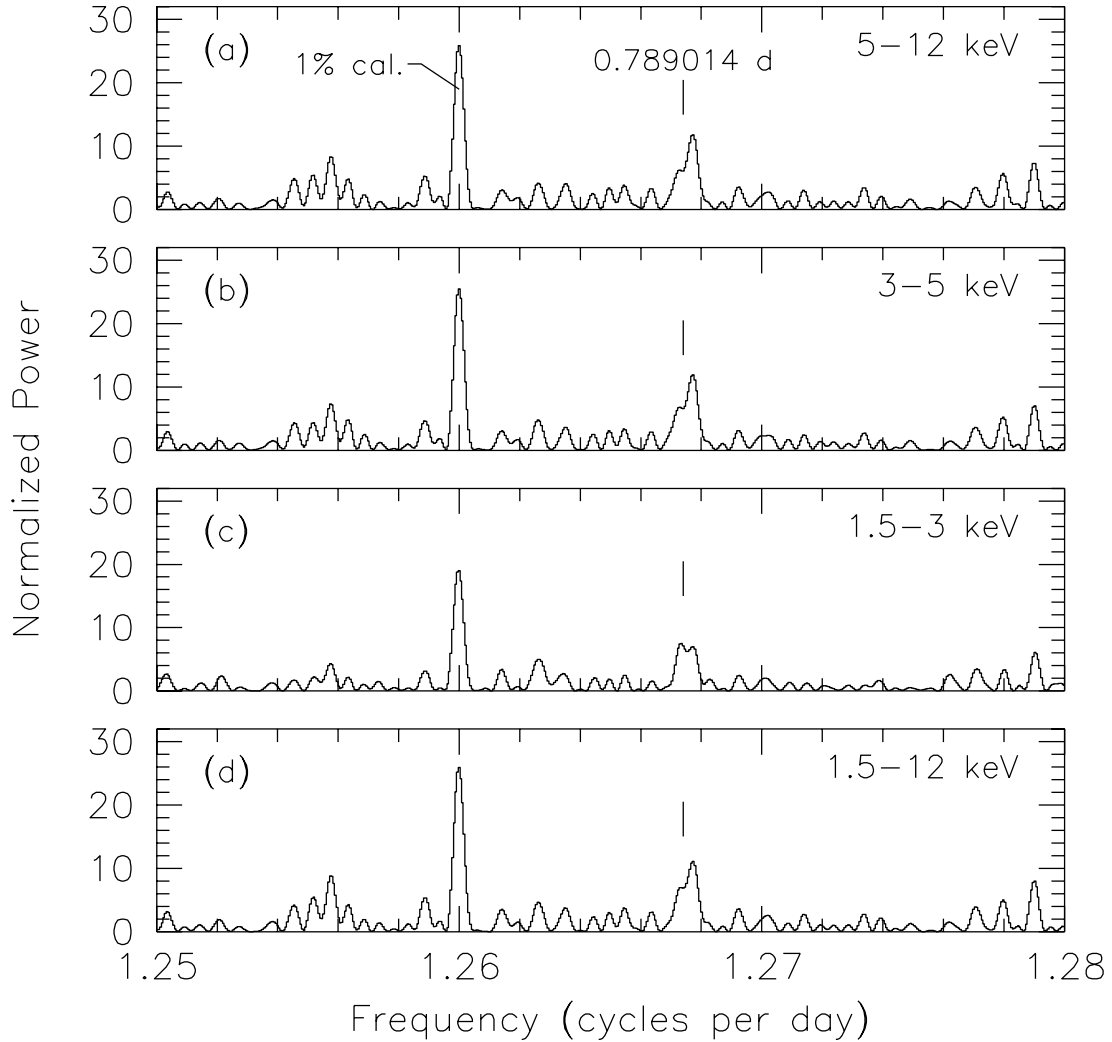


Fig. 5.— (a) Normalized power density spectrum of the corrected SSC 2 C band data to which a sinusoidal signal at a frequency of $1.26 \text{ cycles d}^{-1}$ with a semi-amplitude of 1% (rms amplitude 0.7%) was added in software. A mark indicates the frequency corresponding to a period of 0.789014 days. (b, c, d) Normalized power density spectra for the B, A, and sum bands with 1% calibration signals added.

Table 1. Intensity vs. Hardness Ratio Parameters for SSC 2

Energy Band	α_k	β_k	γ_k	$d \ln F_k / d \ln R_{C,B}^a$
1.5-3 keV (A)	140	100	2.0	1.0
3-5 keV (B)	113	141	2.0	1.3
5-12 keV (C)	50	210	2.5	2.2
1.5-12 keV (sum)	500	280	3.0	1.5

^a $R_{C,B}$ is the 5-12 keV band to 3-5 keV band hardness ratio, and $d \ln F_k / d \ln R_{C,B}$ is given for $R_{C,B} = 1.2$.